

TEMPERATURE DISTRIBUTION OF A TEST SPECIMEN WITH HIGH-SPEED HEAT AIR-FLOW PASSING THROUGH

by

Kai XIONG^a, Yunhua LI^a, and Sujun DONG^{b*}

^a School of Automation Science and Electrical Engineering, Beihang University, Beijing, China

^b School of Aeronautic Science and Engineering, Beihang University, Beijing, China

Original scientific paper

<https://doi.org/10.2298/TSCI160302217X>

In this paper, a solution method for the temperature distribution of rectangular test specimen with a high-speed heat air-flow passing through is proposed based on the heat transfer theory and numerical calculation, and the feasibility of temperature prediction method is validated. Firstly, the partial differential equations to describe the average temperature in the section of the hot air-flow and the specimen are established and the solving method using MATLAB solver is proposed. Then, based on heat transfer conduction equation and the average temperature, the temperature distribution at different point in each section is calculated. The comparison between numerical computation and experiment shows that two results are in good agreement, which verifies the correctness of the presented prediction method of the temperature distribution of the specimen.

Key words: *thermal analysis, high-speed heat air-flow, heat performance prediction*

Introduction

The temperature control on the inner surface of long and narrow rectangle shape test specimen is the key technology of thermal intensity experiments in thermal component of the aero-engine. Because of the harsh environmental condition, narrow installation space, special sensor layout, and high flow temperature and flow rate, the thermal intensity experiments are difficult to be implemented. In most cases, the results of thermal distribution in a test specimen can't be obtained from the experiments, and the numerical calculation method is applied to instead of the experiments. In the case of control the temperature of specimen, the calculation method has theory directive significance to the selection of the control strategy. Therefore, an appropriate accurate method for thermal analysis is very important to obtain the real thermal distributions in test specimen under different conditions.

In this work, the temperature distribution solution of rectangular test specimen will be conducted based on the mechanism analysis and numerical heat transfer method, and the feasibility of temperature prediction solution will be validated.

The thermal analysis of the test specimen with a high speed heat air-flow pass through involves modeling, heat transfer and numerical simulation, and many experts and scholars have done a lot of researches on these fields respectively. Many researchers tend to establish complete mathematical model, and most of them [1-3] use ANSYS to solve the mathematical model. Some

* Corresponding author, e-mail: dsj@buaa.edu.cn

researchers use other methods to solve the mathematical models. Zhang *et al.* [4] proposed a new model and an analytical solution for the heat conduction of tunnel lining ground heat exchangers. The model considered both composite medium and time-dependent boundary, and the analytical solution was obtained by using the superposition principle and finite integral transform method. Based on a series of *quasi-stationary* states, Ferrero and D'Ambrosio [5] presented an alternative approach which utilizes the heat-conduction solver to evolve in a loosely coupled fashion using time steps which are large with respect to the flow time scale. Some researchers analyzed the dynamic process of heat transfer. Wang *et al.* [6] established a thermodynamic model for flow temperature phenomena and presented dynamic temperature compensation by compared the numerical simulations with the experimental measurements. The accuracy and the effectiveness of the compensation method were proved. Ibrahim *et al.* [7] introduced transient modeling of data centers with changing power dissipations and computer room air-conditioning air-flow rates. Transient modeling proved advantageous in monitoring temperature fluctuations. Zohir *et al.* [8] carried out an experimental investigation to study the enhancement in heat transfer coefficient by inserting coiled wire around the surface of the double-pipe heat exchanger inner tube. In order to predicting the heat transfer characteristics of a helical-coiled, crimped, spiral, finned-tube heat exchanger, Boonsri and Wongwises [9] presented theoretical and experimental studies on it, the conclusion shown that the simulation results based on the developed mathematical model agreement with the experimental data.

The study on fluid heat transfer aspects listed as follows. Wae-Hayee *et al.* [10] studied the flow and heat transfer characteristics of in-line impinging jets in cross-flow. The results indicated that Nusselt number peak increased by the increasing cross-flow velocity for short jet-to-plate distance. Hardik *et al.* [11] analyzed the influence of curvature and Reynolds number on local heat transfer coefficient in helical coil with water. Rabari *et al.* [12] investigated the effect of convection heat transfer on performance of waste heat thermoelectric generator. Many researchers [13-15] studied the nature convection, and many researchers focused on the forced convective heat transfer. Aydin *et al.* [16] studied laminar forced convective slip flow in a micro-tube subject with an axially varying heat flux by using the finite volume method. They obtained the conclusion that the mean Nusselt number decreases with an increase in the amplitude. Ashish and Kumarpatil [17] investigated the heat transfer characteristics of grooved fin under forced convection. Elnaggar *et al.* [18] conducted analytical investigations on the horizontal L-shape heat pipe for the laptop-CPU. The 2-D finite element simulation and experimental wall temperatures were found to be a good match. Adesanya *et al.* [19] made the thermodynamic analysis in forced convective flow of a third grade fluid through a vertical channel.

Some researchers [20, 21] studied the problems of thermal structural. Ji *et al.* [20] investigated the bidirectional thermal-structure coupling by using the finite element analysis when the properties of material were temperature-dependent. In order to obtain the high-speed heat air-flow, Li *et al.* [22] and Cai *et al.* [23] studied the oil-fuel supply system and temperature control system of air-flow wind tunnel, respectively, and the control effects were satisfactory. Many numerical simulation of heat transfer were conducted by some researchers [24, 25].

In summary, a lot of effort has been made to performed the thermal analysis of many case, but the thermal analysis of high-speed heat air-flow through the objects are rare. It makes senses to analysis the thermal distribution of a test specimen which has high-speed heat air-flow pass through.

Problem formulation

In order to conduct the thermal strength experiment, the high temperature heat air-flow passes through the thermal specimen is needed. The schematic of thermal test experiment

is shown in fig. 1. Where, the conversion interface temperature is kept at the value of 1000 °C, and the part of test specimen touching with the conversion interface remain 1000 °C. The specimen is insulated with heat preservation material.

The fig. 2 indicates the schematic of test specimen. In the specimen, there are four sensors which positions are shown in fig. 2, and they are used to measure the temperature of point 1, 2, 3, and 4, respectively. The co-ordinates of points 1, 2 and 3 are (0.24, 0.042, 0.060), (0.32, 0.042, -0.065), and (0.48, 0.042, -0.065), respectively. Point 4 is in the middle of the outlet and its co-ordinate are (0.48, 0.042, 0). The sensor in point 4 is used to measure the temperature of outlet air-flow.

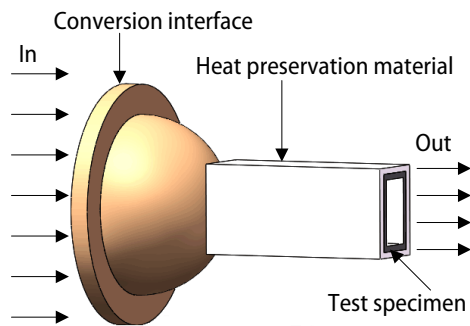


Figure 1. The schematic of thermal test experiment

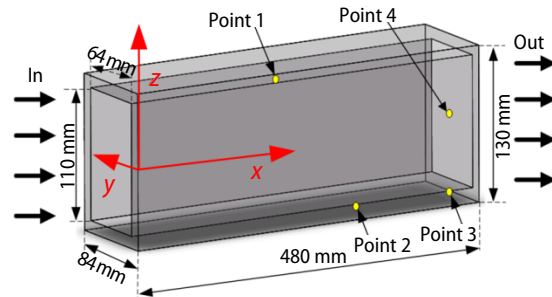


Figure 2. The schematic of test specimen

Mathematic model

This section deals with the establishment of the mathematical model between the sectional average temperature of the air-flow and test specimen, and the temperature distribution in a section of the test specimen.

Heat transfer equation

In order to establish the mathematical model between the temperature of test specimen and air-flow, a segment of test specimen and air-flow along the X-axis is selected to analyze the heat transfer relationship between them. In the process of modeling, the assumptions are described as follows: (1) only the heat convection between the test specimen and heat air-flow is considered, the heat radiation is ignored and (2) there is no heat transfer on the test specimen wrapped by the heat preservation material.

Figure 3 denotes the differential element of the heat transfer. In fig. 3, Φ_f is the inner energy of the fluid in unit time, and Φ_{fx} and Φ_{fs} are the inner energy increment of the air-flow of differential volume and the heat energy absorbed by the test specimen in unit time, respectively.

Considering

$$\Phi_{fx} = \Phi_{f,x-\frac{dx}{2}} - \Phi_{f,x+\frac{dx}{2}} = -c_f \rho_f Q_f \frac{\partial \bar{T}_f}{\partial x} dx, \quad \Phi_{fs} = h_{fs} L_{ct} dx (\bar{T}_f - \bar{T}_s),$$

$$\Phi_f = c_f \rho_f V_f \frac{\partial \bar{T}_f}{\partial t}, \quad V_f = A_{ct} dx, \quad \text{and} \quad Q_f = v_f A_{ct}$$

and substituting them into the energy balance law to the differential volume $\Phi_f = \Phi_{fx} - \Phi_{fs}$ yields:

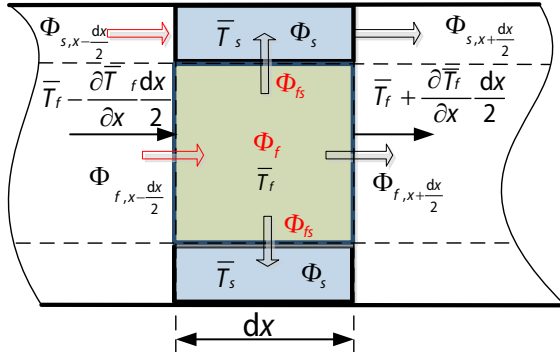


Figure 3. The heart balancing of the airflow and test specimen of the differential volume

$$c_f \rho_f Q_f \frac{\partial \bar{T}_f}{\partial x} dx + c_f \rho_f V_f \frac{\partial \bar{T}_f}{\partial t} = h_{fs} L_{ct} dx (\bar{T}_s - \bar{T}_f) \tag{1}$$

In eq. (1), to write the related coefficients, heat physical parameters, Nusselt number and Reynolds number are:

$$h_{fs} = \frac{\lambda_f}{d} Nu, \quad Nu = 0.023 Re^{0.8} Pr^{0.3} C_t C_l, \quad Re = \frac{v_f d}{\nu}, \quad Pr = \frac{\nu}{a},$$

$$C_l = 1 + \left(\frac{d}{l}\right)^{0.7}, \quad C_t = \begin{cases} \left(\frac{\bar{T}_f}{\bar{T}_s}\right)^{0.5} & \text{The fluid is heated} \\ 1 & \text{The fluid is cooled} \end{cases} \tag{2}$$

$$K_1 = k_1 \frac{1}{c_f \rho_f} \frac{\lambda_f}{\nu^{0.8}} Pr^{0.3} (v_f)^{0.8}, \quad k_1 = 0.023 \left(\frac{1}{d}\right)^{0.2} \left[1 + \left(\frac{d}{l}\right)^{0.7}\right] \frac{L_{cf}}{A_{cf}} = 2.415$$

Substituting eq. (2) to eq. (1) yields:

$$\frac{\partial \bar{T}_f}{\partial t} + v_f \frac{\partial \bar{T}_f}{\partial x} = K_1 (\bar{T}_s - \bar{T}_f) \tag{3}$$

Similar to the derivations of eq. (1) and to define the relative coefficients for the differential volume of test specimen, we can write:

$$\frac{\partial \bar{T}_s}{\partial t} = K_2 (\bar{T}_f - \bar{T}_s) + K_3 \frac{\partial}{\partial x} \frac{\partial \bar{T}_s}{\partial x} \tag{4}$$

where

$$K_2 = \frac{k_2}{c_s \rho_s} \frac{\lambda_f}{\nu^{0.8}} Pr^{0.3} (v_f)^{0.8}, \quad K_3 = \frac{\lambda_s}{c_s \rho_s}, \quad k_2 = 0.023 \left(\frac{1}{d}\right)^{0.2} \left[1 + \left(\frac{d}{l}\right)^{0.7}\right] \frac{L_{cs}}{A_{cs}} = 4.396$$

Equations (3) and (4) are the mathematical model of the test specimen in PDE.

Temperature distribution on the section

We can make the modification for the average temperature of each section along to the thickness of the specimen using the expansion manner in fig. 4. In this way, the analysis of thermal

distribution along the Y- and Z-axis is converted one-dimensional. The temperature along the Z-axis is constant.

The thermal transfer problem of the rectangular elementary body along the Y-axis can be described:

$$\frac{\partial T}{\partial t} = a \frac{\partial^2 T}{\partial y^2} \quad (0 < y < \delta) \quad (5)$$

where $a = \lambda_s / (\rho_s c_s)$, δ – the thickness of the specimen, $\delta = 0.01$, since our focus is temperature variation along y , approximately holds $\partial T / \partial t \approx \partial \bar{T}_s / \partial t$ and eq. (5) can be written:

$$\begin{aligned} \frac{\partial \bar{T}_s}{\partial t} &= a \frac{\partial^2 T}{\partial y^2} \\ \frac{\partial T}{\partial y} \Big|_{y=0} &= 0, \quad \frac{1}{\delta} \int_0^\delta T dy = \bar{T}_s \end{aligned} \quad (6)$$

To solve the PDE expressed by eq. (6) yields the solution:

$$T(y, t) = \frac{1}{2a} \frac{\partial \bar{T}_s}{\partial t} \left(y^2 - \frac{\delta^2}{3} \right) + \bar{T}_s \quad (7)$$

Function fitting

The temperatures of air-flow and test specimen do not keep constant all the time. The thermal properties parameters should be treated as the function of the temperature, such as c_f , ρ_f , ν , λ_f , and c_s , during the process of solving the PDE. Table 1 provides some thermal properties of the standard flue gas under the condition of $P = 101.325$ kPa.

According to the thermal properties in tab. 1, the fitting function of c_f , ρ_f , ν , and λ_f are obtained by using curve fitting tool in MATLAB are:

$$\begin{aligned} \rho_f &= \frac{353}{273 + T_f} \\ c_f &= (-3.787 \cdot 10^{-8} T_f^2 + 2.999 \cdot 10^{-4} T_f + 1.042) \cdot 10^3 \\ \nu &= (4.384 \cdot 10^{-5} T_f^2 + 0.1205 T_f + 2.326) \cdot 10^{-6} \\ \lambda_f &= (8.856 \cdot 10^{-3} T_f + 2.086) \cdot 10^{-3} \\ Pr &= -1 \cdot 10^{-4} T_f + 0.68 \end{aligned} \quad (8)$$

Based on eq. (8), the fitting functions of $Pr^{0.3} \lambda_f / (c_f \rho_f \nu^{0.8})$ and $Pr^{0.3} \lambda_f / \nu^{0.8}$ are obtained, and expressed:

$$\begin{aligned} \frac{1}{c_f \rho_f \nu^{0.8}} Pr^{0.3} \lambda_f &= -2.6486 \cdot 10^{-8} T_f^2 + 1.5368 \cdot 10^{-4} T_f + 0.1432 \\ Pr^{0.3} \frac{\lambda_f}{\nu^{0.8}} &= -1.7435 \cdot 10^{-8} T_f^3 + 7.125 \cdot 10^{-5} T_f^2 - 0.1132 T_f + 156.78 \end{aligned} \quad (9)$$

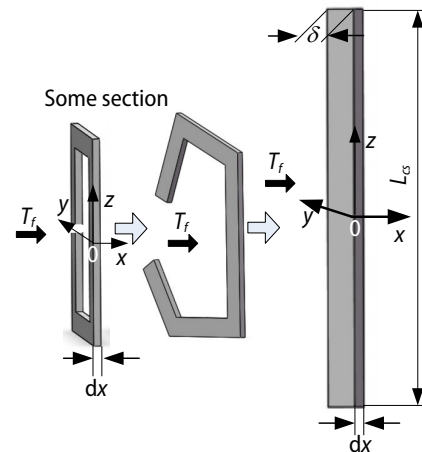


Figure 4. The expansion of some section of the test specimen

Table 1. Some thermal properties of the standard flue gas

T [°C]	ρ_f [kgm ⁻³]	c_f [kJkg ⁻¹ K ⁻¹]	$\nu \cdot 10^6$ [m ² s ⁻¹]	$\lambda_f \cdot 10^2$ [Wm ⁻¹ K ⁻¹]	Pr
300	0.617	1.122	43.9	4.84	0.65
400	0.525	1.151	57.8	5.70	0.64
500	0.457	1.185	73.0	6.56	0.63
600	0.405	1.214	89.4	7.42	0.62
700	0.363	1.239	107	8.27	0.61
800	0.330	1.264	126	9.15	0.60
900	0.301	1.290	146	10.01	0.59
1000	0.275	1.306	167	10.90	0.58
1100	0.257	1.323	188	11.75	0.57
1200	0.240	1.340	211	12.56	0.56
1300	0.225	1.131	234	13.49	0.55
1400	0.211	1.141	258	14.42	0.54
1500	0.199	1.160	282	15.35	0.53
1600	0.189	1.177	307	16.28	0.52
1700	0.179	1.195	333	17.33	0.51
1800	0.170	1.212	361	18.14	0.50

The specific heat of test specimen is shown in tab. 2.

Table 2. The specific-heat of test specimen

T_s [°C]	23	100	200	300	500	700	900	1000	1100	1200	1400
c_s [kJkg ⁻¹ K ⁻¹]	0.75	0.9	1.2	1.25	1.4	1.5	1.65	1.7	1.75	1.8	1.9

To fit for the data in tab. 2 yields the fitting function of c_s as:

$$c_s = (5.974 \cdot 10^{-4} T_s + 1.088) \cdot 10^3 \quad (10)$$

In the simulation computation, $\lambda_s = 10$ W/mK and $\rho_s = 2030$ kg/m³.

The T_f and T_s in eqs. (8) and (9) should be replaced by \bar{T}_f and \bar{T}_s , respectively. The parameters K_1 , K_2 , and K_3 can be calculated:

$$K_1 = (-2.6486 \cdot 10^{-8} \bar{T}_f^2 + 1.5368 \cdot 10^{-4} \bar{T}_f + 0.1432) \cdot 2.415 \nu_f^{0.8}$$

$$K_2 = \frac{-1.7435 \cdot 10^{-8} \bar{T}_f^3 + 7.125 \cdot 10^{-5} \bar{T}_f^2 - 0.1132 \bar{T}_f + 156.78}{(5.974 \cdot 10^{-4} \bar{T}_s + 1.088) \cdot 2.03 \cdot 10^6} \nu_f^{0.8} \cdot 4.396 \quad (11)$$

$$K_3 = \frac{4.9260 \cdot 10^{-6}}{5.974 \cdot 10^{-4} \cdot \bar{T}_s + 1.088}$$

Simulation and analysis

Numerical calculation method based on MATLAB

The pdepe function in MATLAB [26] can solve the partial differential equations, the function call can be written:

$$\text{sol} = \text{pdepe}(m, @\text{pdefun}, @\text{pdeic}, @\text{pdebc}, x, t)$$

where m is a parameter corresponding to the symmetry of the problem, pdefun is a handle that defines the components of the PDE, pdeic is the initial conditions, pdebc is a handle that defines the boundary conditions, x and t are variables.

The PDE model in eqs. (3) and (4) must formulate style of pdefun :

$$c\left(x, t, u, \frac{\partial u}{\partial t}\right) \frac{\partial u}{\partial t} = x^{-m} \frac{\partial}{\partial x} \left[x^m f\left(x, t, u, \frac{\partial u}{\partial t}\right) \right] + s\left(x, t, u, \frac{\partial u}{\partial t}\right) \quad (12)$$

Therefore, the pdefun from PDE can be written:

$$\begin{bmatrix} 1 \\ 1 \end{bmatrix} \cdot * \frac{\partial}{\partial t} \begin{bmatrix} u_1 \\ u_2 \end{bmatrix} = x^0 \frac{\partial}{\partial x} \begin{bmatrix} 0 \\ K_3 \frac{\partial u_2}{\partial x} \end{bmatrix} + \begin{bmatrix} -K_1(u_1 - u_2) - v_f \frac{\partial u_1}{\partial x} \\ K_2(u_1 - u_2) \end{bmatrix} \quad (13)$$

where $u_1 = \bar{T}_f$, $u_2 = \bar{T}_w$. To compare eq. (13) with eq. (12) yields:

$$c = \begin{bmatrix} 1 \\ 1 \end{bmatrix}, \quad m = 0, \quad f = \begin{bmatrix} 0 \\ K_3 \frac{\partial u_2}{\partial x} \end{bmatrix}, \quad s = \begin{bmatrix} -K_1(u_1 - u_2) - v_f \frac{\partial u_1}{\partial x} \\ K_2(u_1 - u_2) \end{bmatrix} \quad (14)$$

The PDE in eqs. (3) and (4) can be solved by the pdepe function in MATLAB [26]. The PDE holds on an interval $0 \leq x \leq 0.48$ for times $t > 0$. The speed of air-flow is $v_f = 0.24 \text{ Ma} = 81.6 \text{ m/s}$. (The Mach number, Ma , is the ratio between the velocity of one point in the field and the local speed of sound.)

The PDE satisfies the initial conditions: $u_1(x, 0) = 1000$, $u_2(x, 0) = 1000$, and boundary conditions:

$$u_1(l, t) = f(t), \quad u_2(0, t) = 1000, \quad \frac{\partial u_2}{\partial x}(l, t) = -\frac{h_{sa}}{\lambda_s}(u_2 - 25)$$

where $f(t)$ is the function of outlet air-flow temperature which change with t , h_{sa} is the convection heat transfer coefficient of test specimen outlet, and equal to 20.

The boundary conditions of the partial derivatives of u must be written in terms of pdebc . The left and right boundary conditions are, respectively:

$$\begin{bmatrix} 0 \\ u_2 - 1000 \end{bmatrix} + \begin{bmatrix} 1 \\ 0 \end{bmatrix} \cdot * \begin{bmatrix} 0 \\ K_3 \frac{\partial u_2}{\partial x} \end{bmatrix} = \begin{bmatrix} 0 \\ 0 \end{bmatrix}, \quad \text{left end} \quad (15)$$

$$\begin{bmatrix} u_1 - f(t) \\ K_3 \frac{h}{\lambda_s}(u_2 - 25) \end{bmatrix} + \begin{bmatrix} 0 \\ 1 \end{bmatrix} \cdot * \begin{bmatrix} 0 \\ K_3 \frac{\partial u_2}{\partial x} \end{bmatrix} = \begin{bmatrix} 0 \\ 0 \end{bmatrix}, \quad \text{right end} \quad (16)$$

where the operator $\cdot *$ indicates Hadamard product in MATLAB [26].

Results and discussion

The object temperature and the adjustment time can be set in the temperature control system of hot wind tunnel. The hot wind tunnel is fired up at 0 s, and the temperature jump to

about 1000 °C. At the same time, the air-flow object temperature of the hot wind tunnel is set to 1050 °C and the adjustment time is set to 400 s. The air-flow temperature is rise to 1050 °C slowly between 0~400 s, and keep at 1050 °C during 400-1400 s. At 1400 s, the target temperature of the hot wind tunnel is set to 1800 °C, and the air-flow temperature began to rise significantly after 1400 s. The outlet air-flow temperature shown in fig. 5 has been measured in point 4 and the fitting curve expressions are described as:

$$f(t) = \begin{cases} 1000 + 0.125t & (0 < t < 400) \\ 1050 & (400 < t < 1400) \\ 1.12 \cdot 10^{-8} t^4 - 1.3858 \cdot 10^{-5} t^3 + \\ + 4.2902 \cdot 10^{-3} t^2 + 0.9591t + 1000 & (1400 < t < 2000) \end{cases} \quad (17)$$

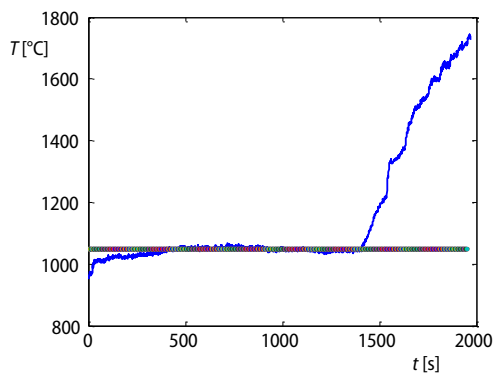


Figure 5. The measurement temperature of outlet airflow

The measurement condition of point 1, 2, 3, and 4 is described as follow: under standard atmosphere, the static press is 100.012 kPa and the total press is 103.983 kPa.

In this paper, the mainly analysis is the process after 400 s and the results displayed is after 800 s. The calculation results of PDE are obtained through the MATLAB differential equation solver. The average temperature of air-flow, \bar{T}_f , and test specimen, \bar{T}_s changing with time and X-axis are shown in fig. 6. According to fig. 6, we can obtain that the heat transfer between the test specimen and heat air-flow is in the steady-state during 400 s to 1400 s and in the dynamic process after 1400 s. The

variation of each section average temperature of test specimen changes along with the each section average temperature of air-flow.

According to fig. 6(a), the air-flow average temperature curves of $x = 0.03$, $x = 0.24$ and $x = 0.48$ are compared in fig. 7(a), We can get the following conclusion: $\bar{T}_f(0.03, t)$, $\bar{T}_f(0.24, t)$, and $\bar{T}_f(0.48, t)$ rise in step, and the temperature difference between any two curves among the three is little in every time.

According to fig. 6(b), the test specimen average temperature curves of $x = 0.03$, $x = 0.24$, and $x = 0.48$ are compared in fig. 7(b). The temperature curves of $\bar{T}_s(0.03, t)$, $\bar{T}_s(0.24, t)$,

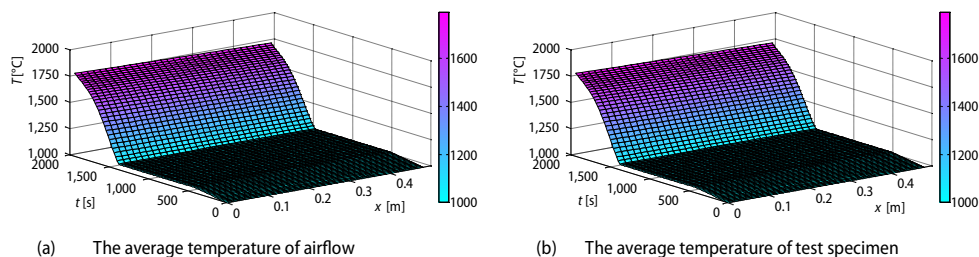


Figure 6. The average temperature changed with time and x
(for color image see journal web site)

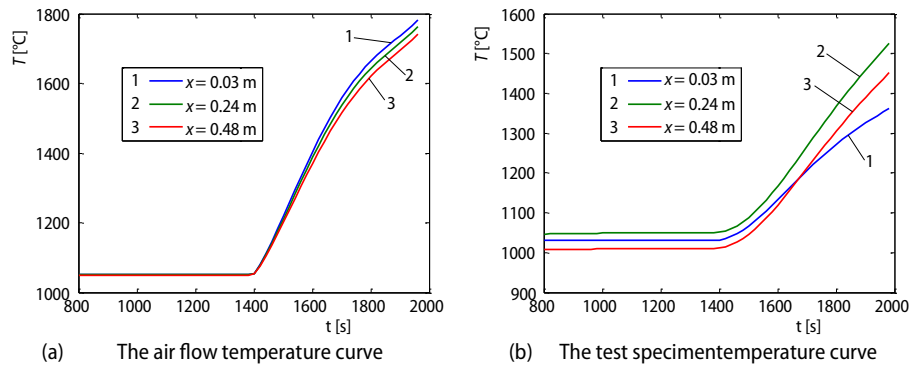


Figure 7. The temperature curve of different section change with time

and $\bar{T}_s(0.48, t)$ all remain the same before 1400 s and rise sharply after 1400 s, in the steady-state, $\bar{T}_s(0.24, t)$ is higher than the other two; because of the inlet ($x = 0$) temperature of test specimen remain in 1000 °C, $\bar{T}_s(0.03, t)$ is lower than $\bar{T}_s(0.24, t)$. Because there is the heat convection at the outlet of the specimen ($x = 0.48$), the $\bar{T}_s(0.24, t)$ is big than the $\bar{T}_s(0.48, t)$.

The temperature curve of every point in the specimen can be calculated through the eq. (7) after $\bar{T}_s(x, t)$ is obtained. The calculated temperature results and measurement results of points 1, 2, and 3 are compared in figs. 8-10, respectively.

In fig. 8, the calculation and measurement results at the point 1 have reached a stable state before 1400 s, while it increases considerably after 1400 s. The difference between the computation and the measurement result is about 20 °C in the steady-state and became larger in the middle of rising stage. In fig. 9, the measurement result obtained before 1760 s is valid for the sensor is broken after 1760 s. The difference between the calculated result and the measurement result is about 30 °C before 1400 s and became larger too in the middle of rising stage. Anyway, the calculated result agrees with the measurement result within the permissible range of error before 1760 s. In fig. 10, before 1400 s, the temperature at the point 3 has reached a stable state; the difference between the calculated result and the measurement result is about 50 °C and the percentage of error is less than 7%. After 1400 s, the temperature at point 3 increases considerably and the calculated result is in accordance with the measurement result.

The percent of difference between calculation result and measurement result is show in fig. 11. In the steady-state, the relative error at points 1, 2, and 3 is less than 5% at most time,

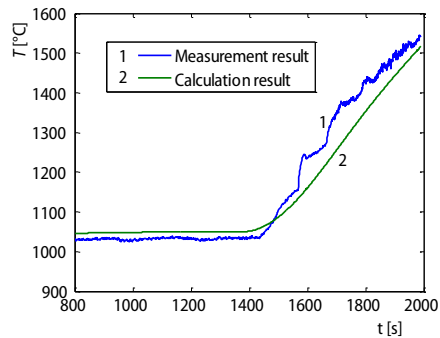


Figure 8. The calculated temperature result and measurement result at point 1

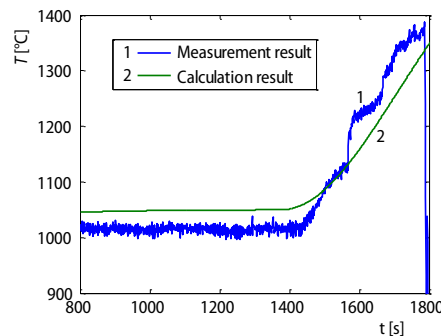


Figure 9. The calculated temperature result and measurement result at point 2

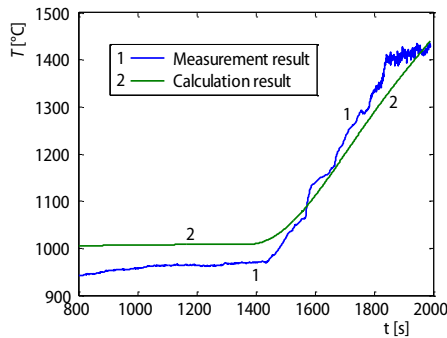


Figure 10. The calculated temperature result and measurement result of point 3

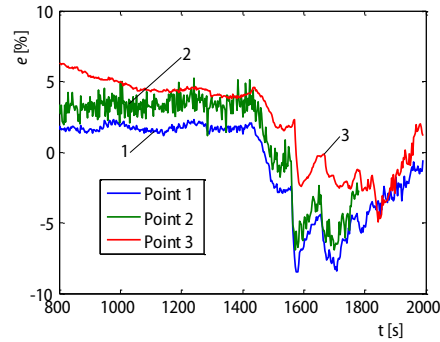


Figure 11. The error percent of point 1, 2 and 3

during the dynamic procedure; the error percent are less than 8% which is acceptable. In the dynamic state, the specific heat capacity of the test specimen is changed with the temperature. While in the process of calculation, the specific heat capacity of test specimen is treated as a constant value which is bigger than the real value in the most time. Hence, the calculation result is smaller than the measurement result. The error between the calculation and measurement in the dynamic state is larger. In steady-state, the heat absorbed equal to the heat dissipated. The change of the specific heat capacity of the test specimen has little influence on the test specimen temperature, and the error in dynamic state is smaller.

Through figs. 8-11, we can get the conclusion: the calculated results are in accordance with the measurement results within an allowed error. It validates the correctness and effectiveness of the model, and reflects that the calculation method has practical value in engineering.

Conclusions

Based on the numerical analysis and the comparison with part of experiments, the conclusions can be summarized as follows.

- The established mathematical model of the specimen with heat air-flow passing through and the proposed solution method via MATLAB solver are available.
- The method described in the paper is applied to temperature prediction, and it can realize that the temperature of every point in the test specimen, under the condition of the outlet temperature of air-flow, the boundary condition and initial condition are known, is able to be calculated. The mathematical model can describe the relationship between the temperature of test specimen and air-flow. When the temperature of a point in the test specimen need to be controlled in a given rang in engineering, the goal can be achieved by adjusting the temperature of outlet air-flow.
- The application of the method provides a prediction method of the temperature distribution of the specimen with heat air-flow passing through, and can be effectively extended to solve the similar problems in engineering.

Nomenclature

A_{ef} – cross section area of air-flow, [m²]
 A_{cs} – cross section area of test specimen, [m²]
 a – intermediate variable
 C_1 – entrance effect correction coefficient
 C_t – temperature difference correction coefficient

c_f – specific heat capacity of air-flow, [Jkg⁻¹K⁻¹]
 c_s – specific heat capacity of test specimen, [Jkg⁻¹K⁻¹]

d	– equivalent diameter of the test specimen, [m]	<i>Greek symbols</i>	
h_{fs}	– he convective heat transfer coefficient between the air-flow and test specimen, [$\text{Wm}^{-2}\text{K}^{-1}$]	δ	– thickness of test specimen, [m]
h_{sa}	– he convective heat transfer coefficient between the air and test specimen, [$\text{Wm}^{-2}\text{K}^{-1}$]	λ_f	– thermal conductivity of heat air-flow, [$\text{Wm}^{-1}\text{K}^{-1}$]
L_{cf}	– outer perimeter of the air-flow, [m]	λ_s	– thermal conductivity of test specimen, [$\text{Wm}^{-1}\text{K}^{-1}$]
l	– length of the test specimen, [m]	ν	– kinematic viscosity of air, [m^2s^{-1}]
Nu	– Nusselt number, [–]	ρ_f	– density of heat air-flow, [kgm^{-3}]
Pr	– Prandtl number, [–]	ρ_s	– density of test specimen, [kgm^{-3}]
Q_f	– flow of heat air-flow, [m^3s^{-1}]	<i>Subscripts</i>	
Re	– Reynolds number, [–]	cs	– cross section of specimen
\bar{T}_f	– sectional mean temperature of heat air-flow, [$^{\circ}\text{C}$]	cf	– cross section of heat air-flow
\bar{T}_s	– sectional mean temperature of test specimen, [$^{\circ}\text{C}$]	f	– air-flow
V_f	– differential volume of the heat air-flow, [m^3]	fs	– air-flow to test specimen
v_f	– velocity of heat air-flow, [ms^{-1}]	l	– length
x, y, z	– co-ordinate system, [m]	s	– specimen
		sa	– test specimen to air
		t	– temperature

References

- [1] Carmona, M., Cortes, C., Analysis of the Thermal Performance and Convection Effects in an Aluminum Holding Furnace Using CFD, *Applied Thermal Engineering*, 76 (2015), 3, pp. 484-495
- [2] Calautit, J. K., *et al.*, CFD and Wind Tunnel Study of the Performance of a Uni-Directional Wind Catcher with Heat Transfer Devices, *Renewable Energy*, 83 (2015), 11, pp. 85-99
- [3] Connor, P. H., *et al.*, Computational Fluid Dynamics Modeling of an Entire Synchronous Generator for Improved Thermal Management, *IET in Electric Power Applications*, 7 (2013), 3, pp.231-236
- [4] Zhang, G., *et al.*, A New Model and Analytical Solution for the Heat Conduction of Tunnel Lining Ground Heat Exchangers, *Cold Regions Science and Technology*, 88 (2013), 4, pp. 59-66
- [5] Ferrero, P., D'Ambrosio, D., A Numerical Method For Conjugate Heat Transfer Problems in Hypersonic Flows, 40th Thermophysics Conference, Seattle, Washington, 2008, pp.23-26
- [6] Wang, C., *et al.*, Thermodynamic Model and Dynamic Temperature Compensation in Positive-Pressure-Based Sonic Nozzle Gas Flow Standard, *IEEE Transactions on Instrumentation and Measurement*, 62 (2013), 5, pp. 1154-1165
- [7] Ibrahim, M., *et al.*, Effect of Transient Boundary Conditions and Detailed Thermal Modeling of Data Center Rooms, *IEEE Transactions on Components, Packaging and Manufacturing Technology*, 2 (2012), 2, pp. 300-310
- [8] Zohir, A. E., *et al.*, Heat Transfer Characteristics in a Double-Pipe Heat Exchanger Equipped with Coiled Circular Wires, *Experimental Heat Transfer*, 28 (2015), 6, pp. 531-545
- [9] Boonsri, R., Wongwiset, S., Mathematical Model for Predicting the Heat Transfer Characteristics of a Helical-Coiled, Crimped, Spiral, Finned-Tube Heat Exchanger, *Heat Transfer Engineering*, 36 (2015), 18, pp. 1495-1503
- [10] Wae-Hayee, M., *et al.*, Flow and Heat Transfer Characteristics of in-Line Impinging Jets with Cross-Flow at Short Jet-To-Plate Distance, *Experimental Heat Transfer*, 28 (2015), 6, pp. 511-530
- [11] Hardik, B. K., *et al.*, Local Heat Transfer Coefficient in Helical Coils with Single Phase Flow, *International Journal of Heat and Mass Transfer*, 89 (2015), 10, pp. 522-538
- [12] Rabari, R., *et al.*, Effect of Convection Heat Transfer on Performance of Waste Heat Thermoelectric Generator, *Heat Transfer Engineering*, 36 (2015), 17, pp. 1458-1471
- [13] Ravník, J., Škerget, L., A Numerical Study of Nanofluid Natural Convection in a Cubic Enclosure with a Circular and an Ellipsoidal Cylinder, *International Journal of Heat and Mass Transfer*, 89 (2015), 20, pp. 596-605
- [14] Kitamura, K., *et al.*, Fluid Flow and Heat Transfer of Natural Convection Adjacent to Upward-Facing, Rectangular Plates of Arbitrary Aspect Ratios, *International Journal of Heat and Mass Transfer*, 89 (2015), 10, pp. 320-332

- [15] Moon, J. Y., *et al.*, Natural Convection Experiments on the Outer Surface of an Inclined Helical Coil, *Heat and Mass Transfer*, 51 (2015), 9, pp. 1229-1236
- [16] Aydin, O., Avci, M., Laminar Forced Convective Slip Flow in a Microduct with a Sinusoidally Varying Heat Flux in Axial Direction, *International Journal of Heat and Mass Transfer*, 89 (2015), 10, pp. 606-612
- [17] Ashish, D., Anil, K. P., Heat Transfer Characteristics of Grooved Fin under Forced Convection, *Heat Transfer Engineering*, 36 (2015), 16, pp. 1409-1416
- [18] Elnaggar, M. H. A., *et al.*, Experimental and Numerical Studies of Finned L-Shape Heat Pipe for Notebook-PC Cooling, *IEEE Transactions on Components, Packaging and Manufacturing Technology*, 3 (2013), 6, pp. 978-988
- [19] Adesanya, S. O., Makinde, O. D., Thermodynamic Analysis for a Third Grade Fluid through a Vertical Channel with Internal Heat Generation, *Journal of Hydrodynamics*, 27 (2015), 2, pp. 264-272
- [20] Ji, Z., *et al.*, Thermo-Plastic Finite Element Analysis for Metal Honeycomb Structure. *Thermal Science*, 17 (2013), 5, pp. 1285-1291
- [21] Bliirken, P., *et al.*, Fast Solvers for Unsteady Thermal Fluid Interaction, *International Journal for Numerical Methods in Fluids*, 79 (2015), 1, pp.16-29
- [22] Li, Y. H., *et al.*, A Novel Cascade Temperature Control System for a High-Speed Heat-Air-flow wind Tunnel, *IEEE-Transactions on Mechatronics*, 18 (2013), 6, pp. 978-988
- [23] Cai, C. Z., *et al.*, Compound Sliding Mode Predictive Control for a Temperature System of High-Speed Heat-Air-flow Wind Tunnel, *Proceedings of the Institution of Mechanical Engineers Part C – Journal of Mechanical Engineering Science*, 228 (2014), 11, pp. 1869-1879
- [24] Udhayakumar, S., *et al.*, Numerical Experiments on the Study of Mixed Convection Flow in Cylindrical Geometry, *Numerical Heat Transfer, Part A*, 68 (2015), 8, pp. 870-886
- [25] Maytorena, V. M., *et al.*, Experimental and Numerical Study of Turbulent Natural Convection in an Open Cubic Cavity, *Heat and Mass Transfer*, 51 (2015), 9, pp. 1205-1217
- [26] ***, MATLAB R2013a User Guide, Mathworks, February 15, 2013